PCCP

PAPER

View Article Online
View Journal | View Issue

Cite this: *Phys. Chem. Chem. Phys.*, 2017, **19**, 20147

Diverse polarization bi-stability in ferroelectric tunnel junctions due to the effects of the electrode and strain: an *ab initio* study†

G. L. Jiang,[ab] W. J. Chen, *[abc] Biao Wang,[c] Jian Shao[ab] and Yue Zheng *[ab]

Received 19th May 2017,
Accepted 5th July 2017

DOI: 10.1039/c7cp03366d

rsc.li/pccp

Both electrodes and substrates are factors of great significance for the performance of ferroelectric tunnel junctions (FTJs) in designing functional nanodevices. To provide a comprehensive view on the polarization stability in FTJs due to the effects of an electrode and a substrate misfit strain, in this work we calculated more than 1000 FTJ structures by utilizing an *ab initio* density functional theory (DFT) method, *via* changing the symmetry of the FTJ structure (*i.e.*, both asymmetric and symmetric FTJs), electrodes (including Au, Ag, Cu, Pt, Co, Fe, and $SrRuO_3$), barrier thickness (ranging from 2 to 10 unit cells), polarization direction (both positive and negative polarizations) and epitaxial strain (*i.e.*, −3%, −2.5%, −2%, −1.5% and −1%) as variables. This shows that the FTJs can exhibit quite diverse polarization bi-stability due to the combined effect of the electrode and strain control, which indicates diverse performance of the FTJs modulated by the electrode and strain. In particular, the polarization-mediated electrostatic potential in the barriers with different electrodes forecasts an electrode-tailored tunnel electroresistance effect. Our study provides guidance on the practical applications of FTJs with regard to the selection of electrodes and substrates.

Introduction

Ferroelectric tunnel junctions (FTJs) combine the quantum-mechanical tunneling effect and switchable spontaneous polarization of a ferroelectric thin film (FTF) to obtain a novel device functionality.[1–3] In an asymmetric ferroelectric tunnel junction (A-FTJ) with different electrodes, the two polarization states are non-equivalent in energy and can be bi-stable only under appropriate conditions. Such bi-stable polarization can be used as a memory state variable,[4,5] and is also the prerequisite of the giant tunnel electroresistance (GER) effect in a FTJ that modulates the tunnel electroresistance by polarization switching[1–3,6,7] or controls the transport spin polarization in a nonvolatile way if the electrodes are ferromagnetic.[8–11]

With its electrode/FTF/electrode sandwich structure, the characteristics of a FTJ depend strongly on the electrode properties and the chemical environment at the interfaces. There are deleterious effects which can reduce a polarization state at the nanoscale and destroy the polarization bi-stability. As is known, a depolarization field can destabilize ferroelectric polarization.[12–14] Using *ab initio* calculations, Junquera and Ghosez[14] investigated the critical thickness of the $SrRuO_3$(SRO)/$BaTiO_3$(BTO)/SRO capacitor and showed that a depolarization field could make the ferroelectricity vanish for BTO films thinner than 6 unit cells. It should be noted that each metal electrode and its conductive oxide electrode have their own screening length. Thus, the depolarization field which comes from the imperfect screening effect can be varied as the electrode changed. In an A-FTJ, the difference between work functions of the two electrode/FTF interfaces can generate an electrostatic field called the built-in field.[15,16] It has been proved that the direction of the built-in field is independent of the polarization state, and it may be in favor of one specific polarization direction and depress the other one.[12,17] Meanwhile, the local chemical environment has been proved to significantly impact the ferroelectric polarization state.[18,19] Stengel *et al.*[18] demonstrated a larger spontaneous polarization in the BTO ultrathin film between Pt electrodes than that in the junctions with Au electrodes. They ascribed this enhancement of the ferroelectric properties to the bonding effect, since TiO_2-terminated BTO can be weakly bonded to the Pt electrode while Au electrodes are more inert. Chen *et al.*[19] presented a comprehensive *ab initio* study on the size effect of symmetric and asymmetric BTO tunnel junctions with Pt and SRO electrodes. The results show that Pt/BTO interfaces have strong coupling with ferroelectric distortion and thus

[a] *State Key Laboratory of Optoelectronic Materials and Technologies, School of Physics, Sun Yat-sen University, Guangzhou 510275, China. E-mail: zhengy35@mail.sysu.edu.cn*
[b] *Micro&Nano Physics and Mechanics Research Laboratory, School of Physics, Sun Yat-sen University, Guangzhou 510275, China*
[c] *Sino-French Institute of Nuclear Engineering and Technology, Sun Yat-sen University, Zhuhai, 519082, China. E-mail: chenweijin@mail.sysu.edu.cn*
† Electronic supplementary information (ESI) available. See DOI: 10.1039/c7cp03366d

play more dominant roles than the SRO/BTO interfaces in affecting the ferroelectric stability of the tunnel junctions. Furthermore, the first-principles and phenomenological modeling by Liu *et al.*[20] predicted that the asymmetric interfaces in SRO/BTO/SRO FTJs induce built-in dipoles at the BaO/RuO_2 interface. These built-in dipoles suppress the polarization when it is pointed towards this interface and lead to a non-switchable polarization for sufficiently thin BTO barriers.[21]

According to the above-mentioned works, both the electrostatic effects and interfacial effects of FTJs are closely connected to the choice of the electrodes. It is natural to wonder as to what happens to the polarization bi-stability of FTJs when we deposit different electrodes in practical situations and what electrode should be chosen in experiment if we want to have an enhanced polarization bi-stability or an enhanced polarization asymmetry, so as to fulfill specific application requirements. In practical applications, electrodes such as Au, Ag, Cu, Pt, Co, Fe, and $SrRuO_3$ are commonly used to fabricate FTJs. Nevertheless, to the best of our knowledge, there have not yet been theoretical or experimental works considering all these electrodes to reveal their delicate effects on the polarization bi-stability of FTJs and to provide a direct comparison.

Besides, applying strain can be another effective means to control the performance of a FTJ.[22–24] It is well known that a substrate misfit strain can enhance the stability of ferroelectricity and can even lead to vanishing of ferroelectric critical thickness. It is also noteworthy that the GER ratio can be enhanced by an applied strain, which has been termed as the giant piezoelectric resistance (GPR) effect.[25] More recently, mechanical switching of ferroelectric polarization has been demonstrated in experiment[26] and by theoretical modeling.[27] Through the so-called flexoelectric effect, the strain gradient exerts an effective electric field to affect the polarization bi-stability. Obviously, the coupling between epitaxial strain and polarization provides a novel perspective for the design of functional devices with FTJs.[28] However, the effect of strain on the polarization bi-stability of FTJs has not been systematically recognized, not to mention the combining effect of strain and electrode. In particular, for A-FTJs, the two polarization states have different stabilities. How does strain modify such stability asymmetry and can this effect play an important role in the mechanical switching of A-FTJs? To answer these questions, research on the combination of electrode-control and strain-control is much-needed and would be promising to provide an additional degree of freedom to control the performance of the FTJs.

In this paper, we reveal the diverse polarization bi-stability in the FTJs with BTO barriers due to the effects of the electrode and strain control. Utilizing the *ab initio* density functional theory (DFT) method, we calculated more than 1000 FTJ structures, *via* changing the symmetry of the FTJ structure (*i.e.*, both asymmetric and symmetric FTJs), electrodes (including Au, Ag, Cu, Pt, Co, Fe, and $SrRuO_3$), barrier thickness (ranging from 2 to 10 unit cells), polarization directions (both positive and negative polarizations) and epitaxial strain (*i.e.*, −3%, −2.5%, −2%, −1.5% and −1%) as variables. The characteristics of the atomic structure, polarization and charge density for these FTJs are revealed and discussed. A concept of an electrode-controlled GPR effect is proposed. We believe that these results will play a guiding role in choosing electrodes and substrates of FTJs in practical situations to meet different application requirements.

Model and methodology

Our basic model and the idea of this work are illustrated in Fig. 1. The FTJs are in a sandwich structure of electrode 1 (at top)/FTF/electrode 2 (at bottom). The screening effect provided by the electrodes is expected to be incomplete, resulting in a residual depolarization field (E_d) that destabilizes the ferroelectric polarization (P) in the barrier. The difference between the work function steps of the two electrode/FTF interfaces generates an electrostatic field called the built-in field (E_{bi}) whose direction is independent of the polarization state. An epitaxial strain is applied by the substrate and we assume that all of the electrode and ferroelectric barrier layers can be fully strained with the substrate. At the M/FTF interface, M–O bonds can be considered as springs whose strength and length will be analyzed and compared in this paper. By choosing different

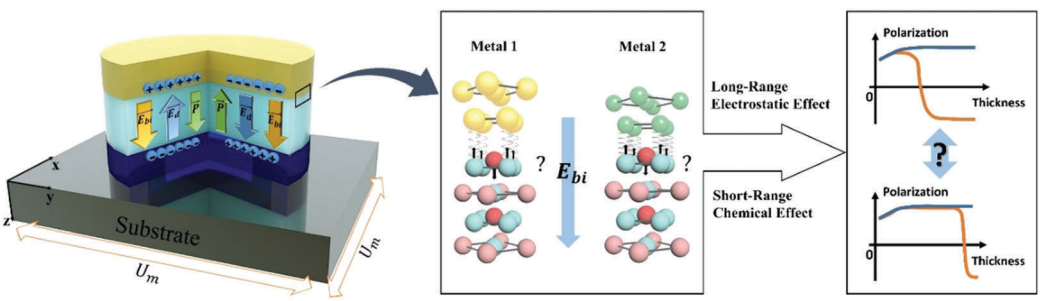

Fig. 1 An asymmetric ferroelectric tunnel junction with a sandwich structure of electrode 1 (at top)/ferroelectric thin film (FTF)/electrode 2 (at bottom) is presented in the left. The screening effect provided by the electrodes is expected to be incomplete, resulting in a residual depolarization field (E_d) which destabilizes ferroelectric polarization (P) in the barrier. The difference between work function steps of the two electrode/FTF interfaces generates a built-in field (E_{bi}). Epitaxial strain is applied by the substrate. At the M/FTF interface, M–O bonds are regarded as springs whose strength and length will be analyzed and compared in this paper. By choosing different electrodes, the polarization bi-stability can be varied as a result of the cooperative or competitive relation between the long-range electrostatic effect and the short-range chemical effect.

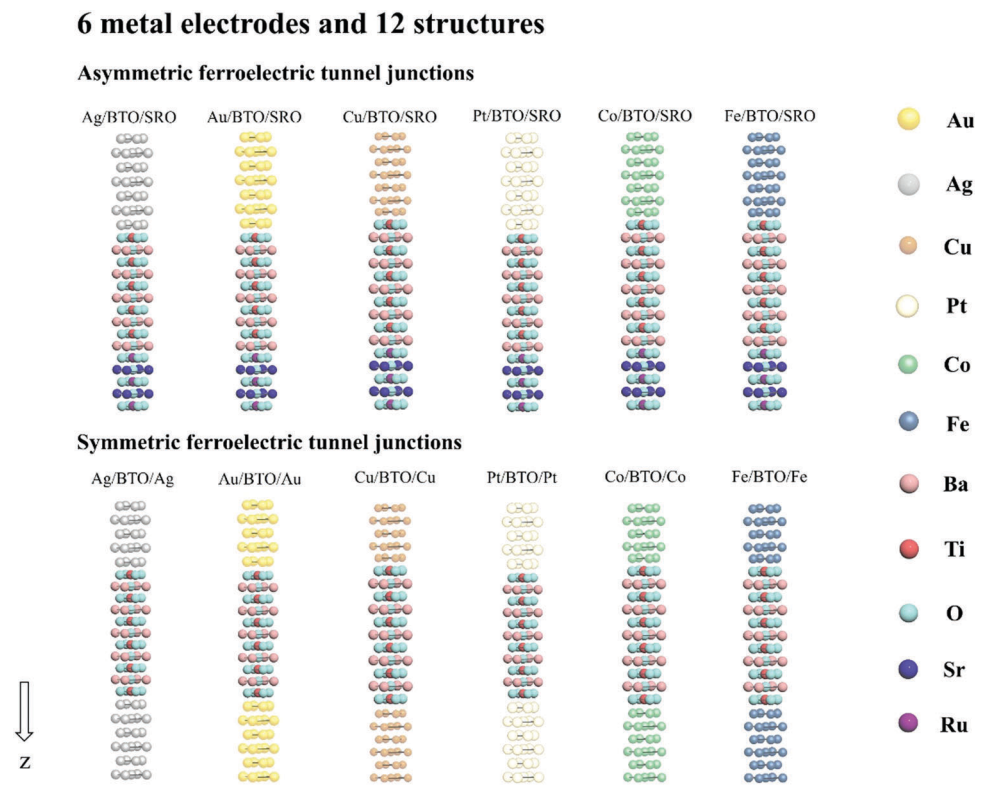

Fig. 2 Schematic atomic structures of the ferroelectric tunnel junctions (FTJs) in our investigation. We calculated more than 1000 FTJ structures in this work. They can be divided into asymmetric FTJs (A-FTJs) and symmetric FTJs (S-FTJs). We choose 6 commonly used metals, Au, Ag, Cu, Pt, Co and Fe as the top electrode and $BaTiO_3$ (BTO) as the ferroelectric barrier. The bottom electrode for the A-FTJs is $SrRuO_3$. In all junctions, the number of BTO layers ranges from 2 to 10. Both positive and negative initial ferroelectric distortions are considered during the calculations. Strain effect is taken into account by further calculating all the A-FTJs and S-FTJs under −3%, −2.5%, −2%, −1.5% and −1% strain.

electrodes, the polarization bi-stability can be varied. This may be the result of the cooperative or competitive relation between the long-range electrostatic effect and the short-range chemical effect.

The calculations in this paper are performed based on the DFT as implemented in the Vienna Ab initio Simulation Package (VASP).[29] A plane-wave basis set and projector augmented wave (PAW) potentials are employed.[30] The exchange correlation potential is treated in the local density approximation (LDA),[31] and the plane wave functions are expanded with an energy cutoff of 500 eV. For structural relaxation, we used a converged $8 \times 8 \times 1$ Monkhorst–Pack grid for k-point sampling[32] with a Gaussian broadening of 0.2 eV. All the atoms are relaxed until the Hellmann–Feynman force on each atom is less than 10 meV $Å^{-1}$.

In our simulations, the FTJs are first modeled to be constrained with an in-plane lattice constant of 3.8273 Å, as −3% strain is being applied. As will be shown later, such a strain can lead to a relatively small critical thickness of polarization bistability for the FTJs. Relaxation of Ag, Cu, Au, Pt, Co, Fe, perovskite BTO (without ferroelectric distortion) and SRO lattices is performed under this in-plane lattice constraint and the relaxed tetragonal unit cells of the bulk Ag, Cu, Au, Pt, Co, Fe, BTO and SRO are then used as building blocks for the supercells. The crystal structures of different metal electrodes used in modeling are (001) oriented face-centered cubic for Ag, Cu, Au, and Pt and (001) oriented face-centered tetragonal for Co and Fe. The top electrode, the BTO ultrathin film and bottom electrode layers are stacked along the [001] direction (*i.e.*, z-direction) of the bulk counterparts. Therefore, the supercells are considered in the perpendicular direction to the transport direction. The short-circuit boundary condition is naturally introduced by constructing a superlattice under periodic boundary conditions. Based on the relaxed structure of the supercells under −3% strain, we then change the in-plane lattice constant to apply different strain conditions including −2.5%, −2%, −1.5% and −1% strain to the supercells. A strain-application process can thus be mimicked, and the strain effect on the polarization bi-stability in the FTJs with a tetragonal phase of the ferroelectric barrier can be revealed.

To give a comprehensive insight into the mechanism of electrode control, we first constructed completely asymmetric structures (with different electrodes and combinations of terminations) for simulations, *i.e.*, $M/(TiO_2–BaO)_m/SRO$ (M = Ag, Cu, Au, Pt, Co and Fe), with the number of perovskite unit-cells m ranging from 2 to 10 for each type of tunnel junctions, as can be seen in the first row of Fig. 2. The TiO_2 termination is chosen because it is more energetically preferable than BaO terminations according to previous reports on interfacial work.[19] To eliminate the effect of electrode thickness, 9 monolayers of metal atoms and seven monolayers of SRO electrodes have been considered. For comparison, we also simulate the completely symmetric structure

M/(TiO_2–BaO)$_m$–TiO_2/M (with identical electrodes and terminations) with six and seven monolayers in each electrode. The schematic macrostructures of the S-FTJs calculated are depicted in the second row of Fig. 2. Overall, there are seven interfacial configurations provided, and the total number of FTJs to be calculated is 2 (two polarization directions) × 9 (BTO unit-cell layers m ranging from 2 to 10) × 6 (the number of metal electrodes) × 5 (five strain states) × 2 (asymmetric and symmetric FTJs) = 1080.

It is necessary to note that, in A-FTJs the metal electrode is labeled as electrode 1 and SRO is labeled as electrode 2. The z-direction pointing from electrode 1 to electrode 2 is defined as positive. $P_0\rightarrow$ and $P_0\leftarrow$ represent the positive and negative initial ferroelectric polarization, respectively. In the S-FTJs, electrode 2 is replaced by a metal. To find out the preference in polarization stability, we first impose negative initial displacements of Ti atoms along the [001] direction with respect to the O atoms in the same x–y plane, and then fully relax all of the atoms in the supercell to find out whether this negative state can be maintained. Junctions with positive initial displacements of Ti atoms are also simulated when their negative polarization can exist stably. The Berry phase method[33] is utilized to calculate the local polarization P of the FTJs according to the formula $P = e\sum z_i^* u_i / V$, where e is the electronic charge, z_i^* is the Born effective charge of the ion i, u_i is the displacement of the ion i in the ferroelectric state with respect to the paraelectric state and V is the volume of the unit cell. Using the Berry phase method, the calculated Born effective charges are 2.85 and 5.27 for Ba and Ti, respectively, and −4.26 and −1.91 for O in the BaO and TiO_2 planes, respectively.[34]

Results and discussion

A. The short-range effect of the metal–oxygen bond

We first study how different metal electrodes influence the polarization bi-stability of the A-FTJs. The discussion will mainly focus on the interfacial states from the viewpoint of energy. Fig. 3 depicts the parabolic relationship between the M–O bond energy and the M–O bond length for M/(TiO_2–BaO)$_9$/SRO asymmetric ferroelectric junctions under −3% strain to evaluate the M–O bond strengths. We expect some correlation between the M–O bond strengths and the polarization bi-stability. Shown in Fig. 3(a–f) are the results of Ag/(TiO_2–BaO)$_9$/SRO, Cu/(TiO_2–BaO)$_9$/SRO, Au/(TiO_2–BaO)$_9$/SRO, Pt/(TiO_2–BaO)$_9$/SRO, Co/(TiO_2–BaO)$_9$/SRO and Fe/(TiO_2–BaO)$_9$/SRO, respectively. As can be seen in Fig. 3, all the M–O bonds have two curves for both positive and negative polarizations, except for Ag–O and Cu–O bonds as the negative polarization does not show up in Ag/(TiO_2–BaO)$_9$/SRO and Cu/(TiO_2–BaO)$_9$/SRO junctions. So we mainly compared the bond strength among junctions with positive polarization. Note that with the same change in bond length d, the more free energy increases, the stronger the bond is. We can evaluate bond strength visually in Fig. 3 that within the same range of the abscissa axis, the results of Ag/(TiO_2–BaO)$_9$/SRO, Cu/(TiO_2–BaO)$_9$/SRO and Au/(TiO_2–BaO)$_9$/SRO each present a wider parabola compared with Pt/(TiO_2–BaO)$_9$/SRO, Co/(TiO_2–BaO)$_9$/SRO and Fe/(TiO_2–BaO)$_9$/SRO junctions. To give a quantitative comparison, we consider the M–O bond as a spring and calculate the bond strength as k in the following form as $E = k\Delta d$. The value of k is listed in Table 1. Apparently, the

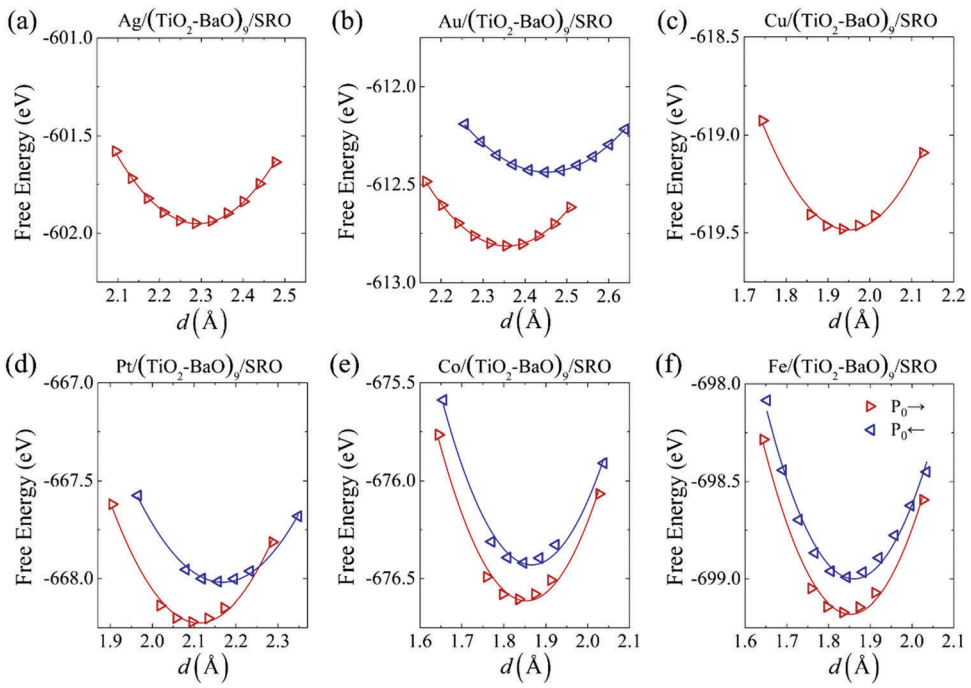

Fig. 3 The parabolic relationship between the M–O binding energy and the bond length for the M/(TiO_2–BaO)$_9$/SRO A-FTJs under −3% strain. (a–f) The results of Ag/(TiO_2–BaO)$_9$/SRO, Cu/(TiO_2–BaO)$_9$/SRO, Au/(TiO_2–BaO)$_9$/SRO, Pt/(TiO_2–BaO)$_9$/SRO, Co/(TiO_2–BaO)$_9$/SRO and Fe/(TiO_2–BaO)$_9$/SRO, respectively. All the M–O bonds have two curves for both positive (red) and negative (blue) polarization, except for the Ag–O bond and the Cu–O bond as the negative polarization does not show up in Ag/(TiO_2–BaO)$_9$/SRO and Cu/(TiO_2–BaO)$_9$/SRO junctions.

Table 1 Calculated bond strength k of the M–O bond and the D-value for the A-FTJs. Since the negative polarization do not show up in the Ag/(TiO_2–BaO)$_9$/SRO and Cu/(TiO_2–BaO)$_9$/SRO junctions, their D-values are not available

	Ag	Au	Cu	Pt	Co	Fe
K	8.816	9.209	12.943	13.798	18.903	20.057
D-value (eV)	—	0.37	—	0.20	0.19	0.18

bonds Ag–O and Au–O can be classified into one group with weaker bond strength while the bonds Co–O and Fe–O belong to the stronger ones. The bonds Cu–O and Pt–O are in the middle. For a strong M–O bond (here we denote it as M_s–O while M_w–O for a weak bond), more energy is needed to reverse the initial negative polarization to a positive state, so M_s/(TiO_2–BaO)$_9$/SRO junctions are more likely to maintain a negative state. Note that the interface at the SRO electrode is BaO/RuO_2 in the modeled FTJs. We have listed the interfacial information in Table S1 (ESI†), including the distance between Ru–O′, Ba–O′ and Ru–O″ of M/(TiO_2–BaO)$_9$/SRO with positive initial polarization and −3% strain, where O′ and O″ denote the oxygen atoms in BaO and RuO_2, respectively. The differences of the BaO/RuO_2 interface structure among different tunnel junctions are small (about 0.1 Å).

The formation of the M–O bond is essential to the charge transfer at the interface. To analyze the charge transfer of M–O bonds at the interface, we further investigated the differential electron charge density $\Delta\rho_{scf\text{-}nscf}$, which denotes the difference in charge densities between those obtained from a self-consistent calculation and a non-self-consistent calculation (*i.e.*, a superposition of atomic electron charge densities). Fig. 4 depicts $\Delta\rho_{scf\text{-}nscf}$ distributions (cut at the middle [100] or [110] plane of the supercell) at the M/TiO_2 interfaces of all six A-FTJs with m = 9 and a positive polarization pointing to the metal. For comparison, we also calculated the cases with a negative polarization (pointing to the BTO film), see Fig. S1 (ESI†), where electron loss is shown in blue color and electron gain in red color. Oxygen atoms tend to gain electrons from the other atoms after bonding, while both Ba atoms and M atoms are inclined to lose electrons. As can be seen, the charge density increases more at the interface of Co/TiO_2 and Fe/TiO_2, implying a strong bonding between Co (or Fe) and O atoms while the amount of charge transferred is moderate at the interface of Cu/TiO_2 and Pt/TiO_2, and it is even smaller at the interface of Ag/TiO_2 and Au/TiO_2. The shape of the electron clouds around O and Ti atoms suggests the p_z characteristic of the orbitals for the oxygen and the d_{xz} (d_{yz}) characteristic for the titanium.[35] The electron clouds of the electrodes present two kinds of shapes, dividing the metals into two types, a pancake shape for Ag, Au and Cu while a dumbbell shape for Pt, Fe and Co. These results are in accordance with the above-mentioned classification based on the metal electrodes.

B. The long-range electrostatic effect

From the view of free energy, the two directions of polarization share an unequal energetic preference in an A-FTJ. In Fig. 5, we plot the double-well profile for the six asymmetric structures with 9 layered unit cells of BTO to give a comparison. Still there are only results with a positive polarization for Ag/(TiO_2–BaO)$_9$/SRO and Cu/(TiO_2–BaO)$_9$/SRO junctions due to the absence of a negative polarization state. From the results of Au/(TiO_2–BaO)$_9$/SRO, Pt/(TiO_2–BaO)$_9$/SRO, Co/(TiO_2–BaO)$_9$/SRO and Fe/(TiO_2–BaO)$_9$/SRO, the negative state is higher in energy and has a smaller effective barrier height for reversal than the positive polarization state. This difference indicates a positive built-in

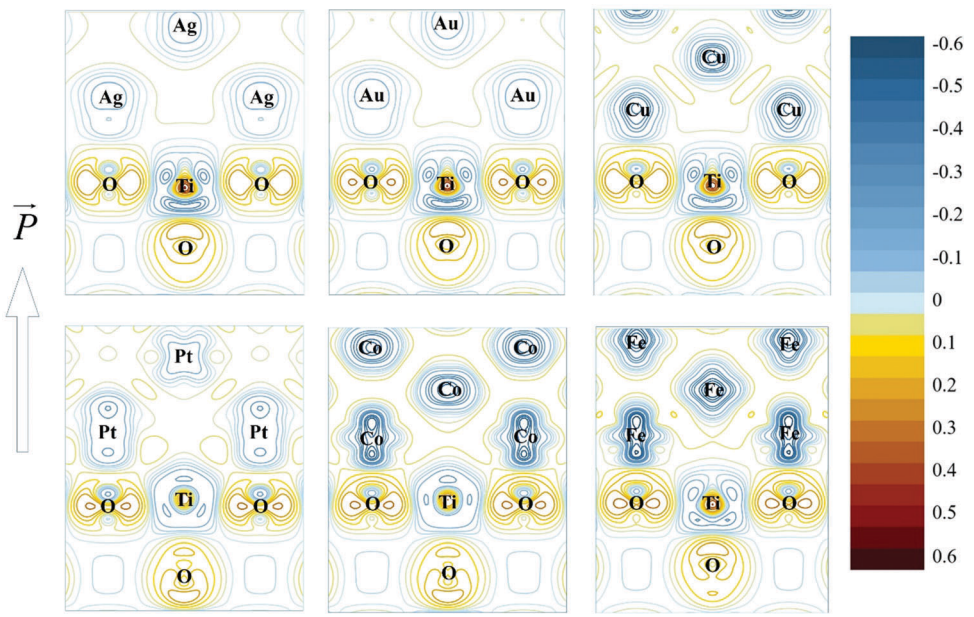

Fig. 4 Calculated differential charge density profile at the relaxed interfaces of the M/(TiO_2–BaO)$_9$/SRO A-FTJs. The tunnel junctions are in the ferroelectric state with the direction of the polarization as indicated by the arrow. Electron loss is shown in the blue color and electron gain in the red color.

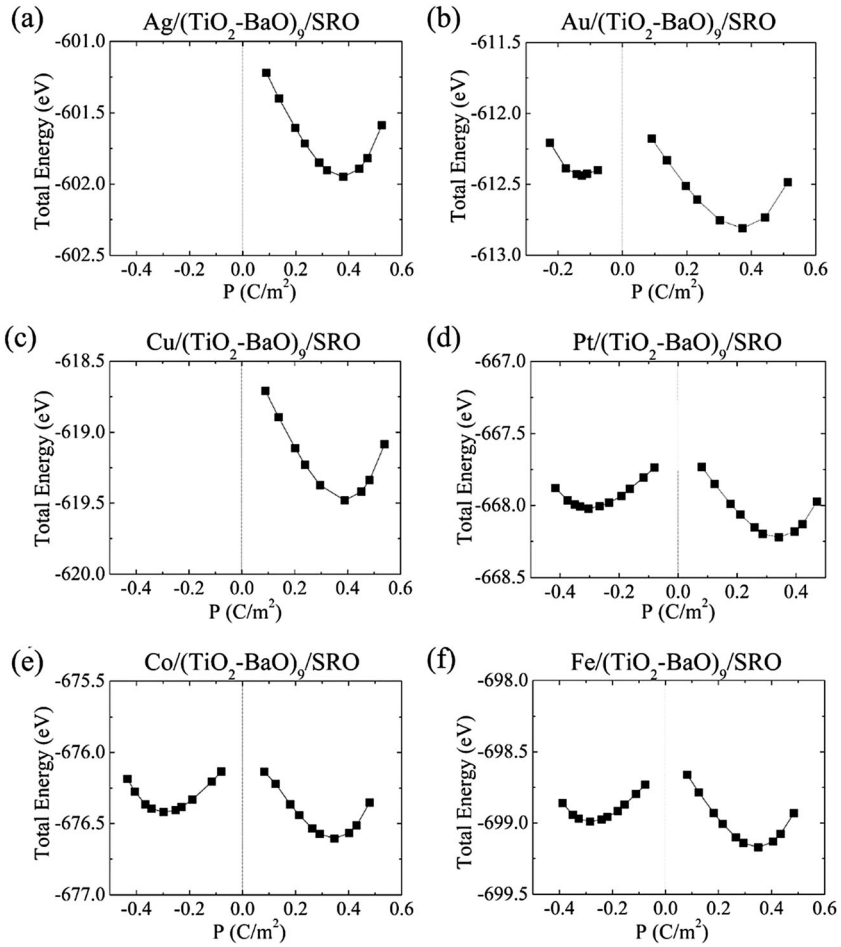

Fig. 5 Double-well total energy profile of the six M/(TiO_2–BaO)$_9$/SRO A-FTJs under −3% strain. For Ag/(TiO_2–BaO)$_9$/SRO and Cu/(TiO_2–BaO)$_9$/SRO junctions, there is only the result with the positive polarization due to the absence of their negative polarization state.

field existing in the BTO barrier which makes the positive polarization energetically more preferable. At the beginning of our model with a negative initial ferroelectric distortion, the O atoms at the interface are in a relatively distant location from the metal atoms. The elongated M–O bond has to compete with this built-in field to reach a steady state of minimum energy. In this competitive relation, weaker bonds like Ag–O and Au–O might be dragged to be shorter, supporting the polarization reversal to the positive state, whereas Pt/(TiO_2–BaO)$_9$/SRO, Co/(TiO_2–BaO)$_9$/SRO and Fe/(TiO_2–BaO)$_9$/SRO junctions could possibly hold the negative polarization with a smaller critical thickness. It is worth noting that among these four polarization bi-stable junctions, the energy profile of Au/(TiO_2–BaO)$_9$/SRO is relatively special. For an explanation, the difference in value (*D*-value) between the two minimal energies in one junction is listed in Table 1, which shows that the *D*-value of Au/(TiO_2–BaO)$_9$/SRO is 0.37 eV, higher than those of the others, leading to a more unfavorable negative state in it. Hence, in addition to the different atomic bonds at the interfaces, the electrode tuning of energy difference also leads to further asymmetry of the ferroelectric stability. The above results tend to classify the six metal electrodes into two types: junctions with Ag, Cu and Au electrodes (M_w) show more inhibition for a negative polarization while it is easier for those with Pt, Co and Fe electrodes (M_s) to remain in bi-stable polarization. This trend is more intuitive when analyzing the interfacial structure. A series of computed structural parameters at the M/FTF interfaces of M/(TiO_2–BaO)$_9$/SRO junctions are depicted in Fig. S2 (ESI†).

C. Polarization bi-stability in asymmetric ferroelectric tunnel junctions

The local polarization distribution of the six types of asymmetric tunnel junctions is shown in Fig. 6, where (a), (b), (c), (d), (e) and (f) label the results of Ag/(TiO_2–BaO)$_m$/SRO, Cu/(TiO_2–BaO)$_m$/SRO, Au/(TiO_2–BaO)$_m$/SRO, Pt/(TiO_2–BaO)$_m$/SRO, Co/(TiO_2–BaO)$_m$/SRO and Fe/(TiO_2–BaO)$_m$/SRO tunnel junctions, respectively, with m ranging from 2 to 10. The layer index is set zero at the middle plane of the barrier. As shown in Fig. 6(a and c), choosing Ag and Cu as top electrodes will lead the tunnel junctions to present a positive polarization state even when m is up to 10. In Fig. 6(b), the Au/(TiO_2–BaO)$_m$/SRO junctions exhibit a critical thickness of m = 9. What is noteworthy is that when m = 9 or 10, the polarization in the BTO unit cells near the Au/BTO interface points to an opposite direction compared with the rest of unit cells

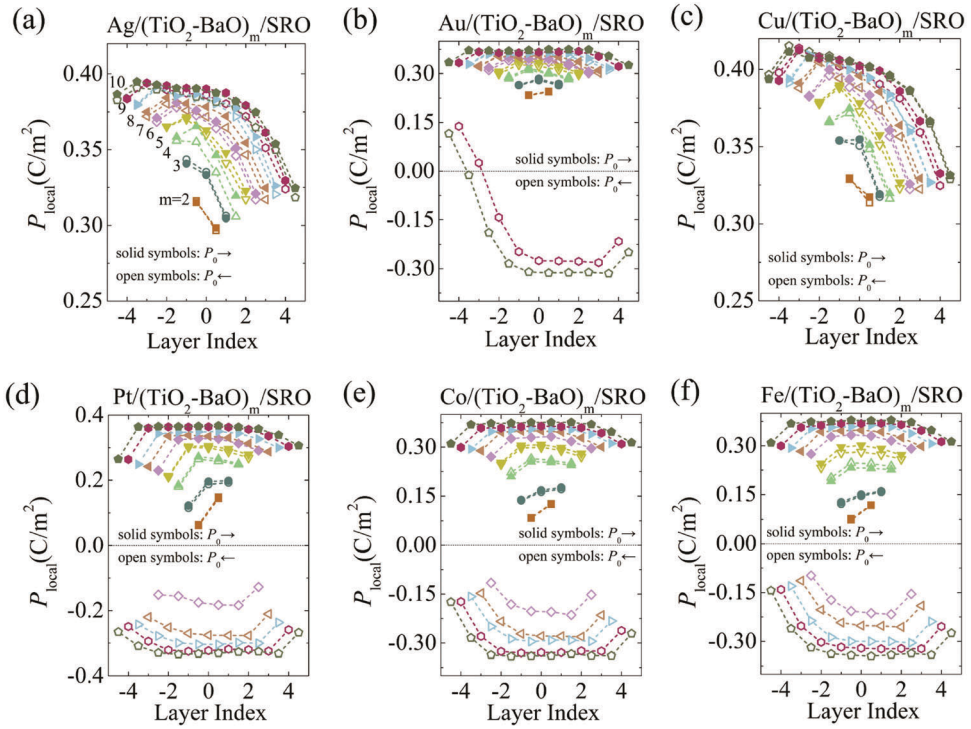

Fig. 6 The local polarization distribution of the six M/(TiO_2–BaO)$_m$/SRO A-FTJs with m ranging from 2 to 10 under −3% strain. The layer index is set zero at the middle plane of the barrier.

that remain in negative polarization. Such an interfacial pinning behavior can be ascribed to the weak Au–O bond which is easily dragged by the built-in field. Although the Au/BTO interfacial structure changes, the initial negative polarization still remains. As for the tunnel junctions covering M_s electrodes, *i.e.*, Pt, Co and Fe, an enhanced polarization bi-stability is observed, with the critical thickness of polarization bi-stability being m = 6. These results are in accordance with the interfacial bonding analysis. Fig. 7 summarizes the average polarization as a function of unit-cell number m, where Fig. 7(a and b) depict the results for A-FTJs with positive and negative initial polarization, respectively. We can evaluate the ferroelectricity in Fig. 7(a) since the junctions are uniformly relaxed to a positive polarization state. The polarization is up to 0.39 C m^{-2} for the case of Cu electrode, while the polarization of the Pt/(TiO_2–BaO)$_m$/SRO junction is the smallest.

D. Epitaxial strain effect

For the purpose of revealing how the strain affects the polarization bi-stability and to combine the strain control with an electrode control, we decrease the substrate strain to see if there is a change in the polarization state. Fig. 8(a–f) present the average polarization of Ag/(TiO_2–BaO)$_m$/SRO, Cu/(TiO_2–BaO)$_m$/SRO, Au/(TiO_2–BaO)$_m$/SRO, Pt/(TiO_2–BaO)$_m$/SRO, Co/(TiO_2–BaO)$_m$/SRO and Fe/(TiO_2–BaO)$_m$/SRO, respectively, with strain ranging from −3% to −1%. Since the positive polarization state will always show up when m < 6, here we only present the results with m ranging from 6 to 10 to highlight the strain effect on polarization bistability in the FTJs in this thickness range. In Ag/(TiO_2–BaO)$_m$/SRO and Cu/(TiO_2–BaO)$_m$/SRO junctions, the polarization gradually increases with decreasing compressive strain. Besides, the critical thickness of the negative polarization

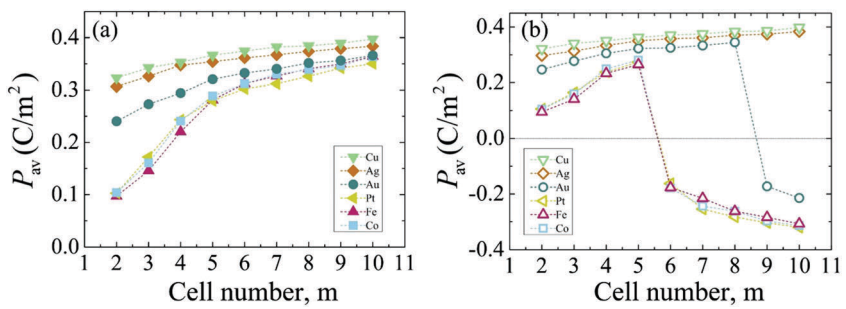

Fig. 7 The average polarization as a function of unit-cell number m for the M/(TiO_2–BaO)$_m$/SRO A-FTJs: (a) with the positive initial polarization and (b) with the negative initial polarization, respectively.

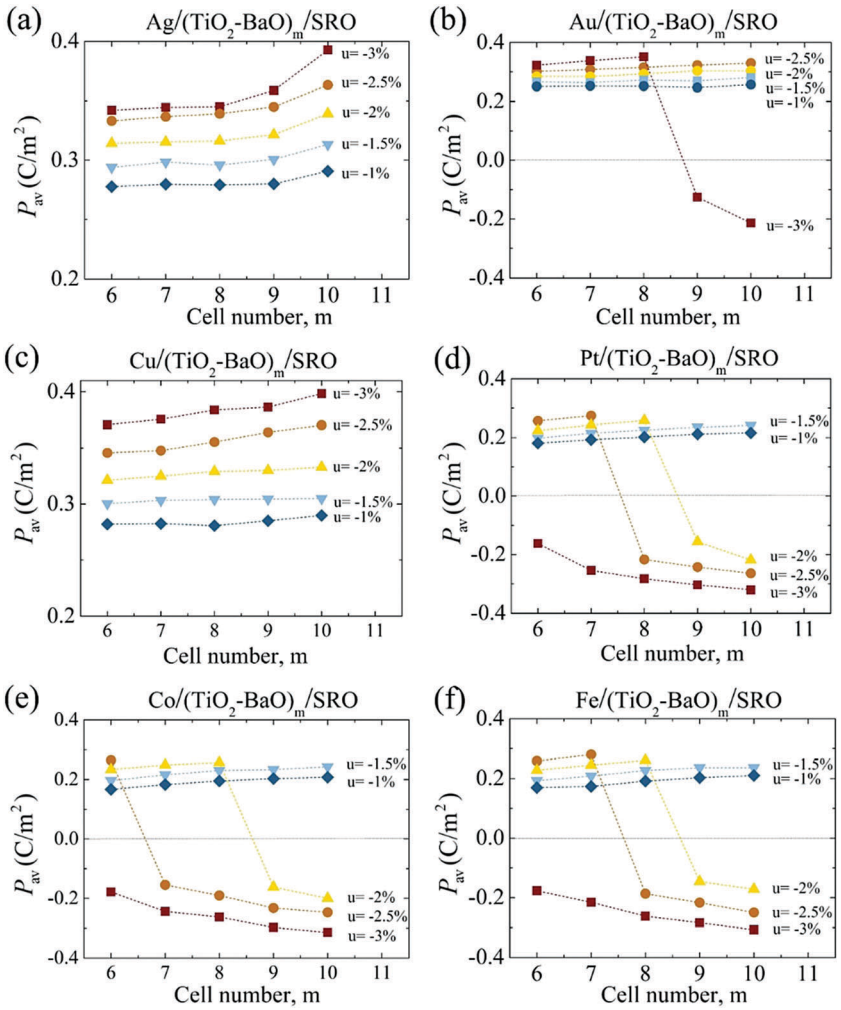

Fig. 8 The average polarization of the M/(TiO_2–BaO)$_m$/SRO A-FTJs with m ranging from 6 to 10 and strain ranging from −3% to −1%.

state in Au/(TiO_2–BaO)$_m$/SRO, Pt/(TiO_2–BaO)$_m$/SRO, Co/(TiO_2–BaO)$_m$/SRO and Fe/(TiO_2–BaO)$_m$/SRO has the same variation trend. To give an intuitionistic picture of the combining effect of electrode and strain, we further summarize the critical thickness of the negative polarization state under different applied strains with all six metal electrodes, as depicted in Fig. 9. This result shows the minimum barrier thickness for different A-FTJs to preserve polarization bistability and can be a guide for experiments. For example when a −3% strain substrate and M_s electrodes are chosen, 2.7 nm is enough for the deposited BTO thin film to carry out bi-stable polarization. However, the barrier has to be thicker than 4 nm to maintain the polarization bi-stability when the epitaxial strain is less than or equal to −2%, or when the Au electrode is chosen. The combined electrode control and strain control thus allows more flexible change in the polarization state in the FTJs.

We would like to point out that such a strain-dependent polarization bistability of the A-FTJs shown in Fig. 8 and 9 indicates a possibility of 'mechanical switching' of the metastable polarization state. For the A-FTJs investigated here, the metastable polarization state is the negative polarization state.

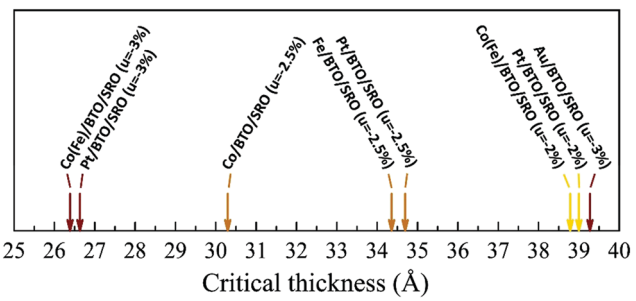

Fig. 9 An intuitive picture of the double control of the electrode and strain control, summarizing the critical thickness of the negative polarization state under a different applied stain with all six metal electrodes.

This state can maintain stability at a relative compressive strain state; however, it would become unstable at a relative tensile strain state due to an increase in the critical thickness of polarization bistability. For example, as shown in Fig. 8d, the negative polarization state is stable in the Pt/(TiO_2–BaO)$_6$/SRO junction at a strain of −3%, but it cannot maintain stability at a strain of −2.5% and is relaxed into the positive state.

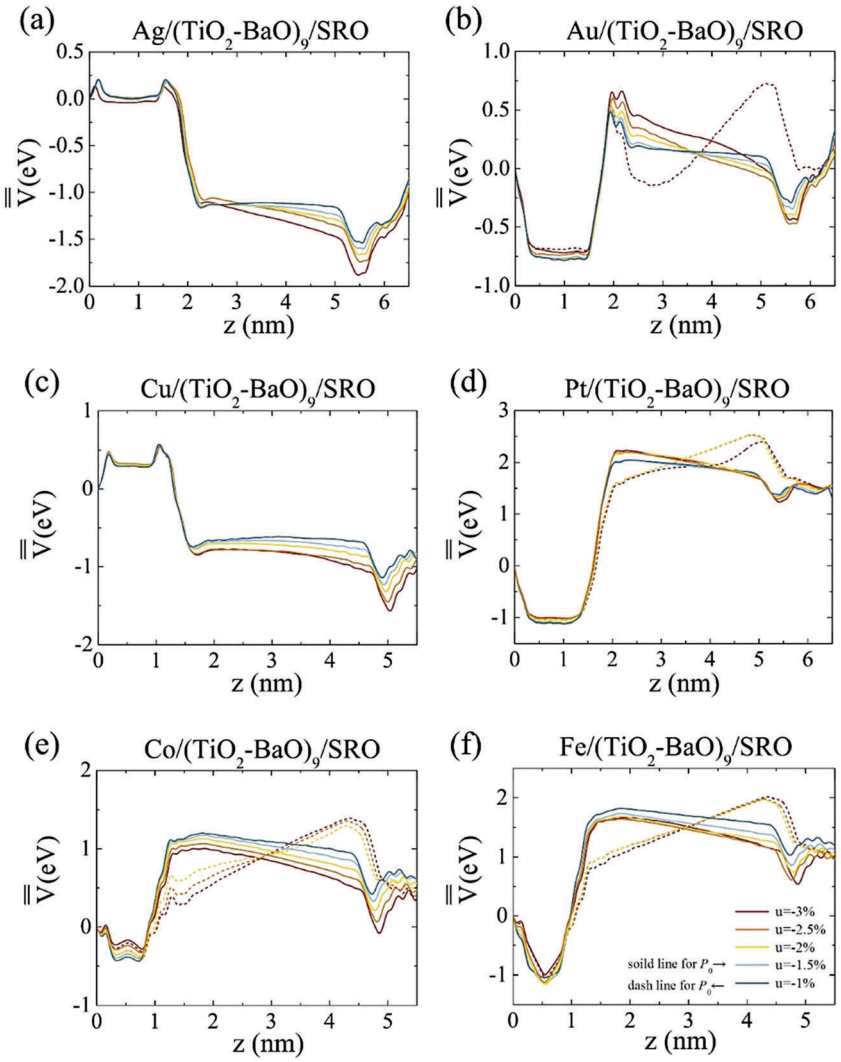

Fig. 10 The strain-dependent macroscopic-averaged electrostatic potential energy profile along the z-direction $\overline{\overline{V}}(z)$ for the M/(TiO_2–BaO)$_9$/SRO A-FTJs in both positive and negative polarization states. The strain ranges from −3% to −1%.

Therefore, switching of the metastable polarization state can occur if the strain state of the FTJ can be controlled. In practice, the epitaxial strain is fixed once the film was grown on a substrate. Nevertheless, a relatively tensile strain might be exerted to the FTJs by a local tip force. Depending on the FTJ layer stacking sequence, it is expected that such a strain effect on polarization bistability can either promote or offset the flexoelectric switching in A-FTJ systems.

The strain-dependent macroscopic-averaged electrostatic potential energy profile along the z-direction $\overline{\overline{V}}(z)$ for the A-FTJs with m = 9 in both positive and negative polarization states is depicted in Fig. 10. With asymmetric interfaces, non-centrosymmetric potential profiles are expected. Firstly, we make comparisons among different metal electrodes under −3% strain. A depolarization field is found in the barriers of all tunnel junctions due to the appearance of net polarization. Among junctions with a positive polarization, a largest depolarization field of about -2.03×10^8 V m^{-1} is found in the barrier of the Pt/(TiO_2–BaO)$_9$/SRO junction while the smallest depolarization field of about -0.98×10^8 V m^{-1} is found in the barrier of the Cu/(TiO_2–BaO)$_9$/SRO tunnel junction. This result is identical to that shown in Fig. 7(a), which indicates the largest polarization in Cu/(TiO_2–BaO)$_9$/SRO and the smallest polarization in the Pt/(TiO_2–BaO)$_9$/SRO junction. Note that there are significant potential peaks at M_w/TiO_2 interfaces. This also separates Ag, Au and Cu from the M_s electrodes. Among the tunnel junctions with negative polarization, the depolarization field in the barrier of Au/(TiO_2–BaO)$_9$/SRO has a special reversal at the interface of Au/TiO_2 which is in accordance with the pinning behavior mentioned above. For M_s/(TiO_2–BaO)$_9$/SRO junctions, the total electric field within the barrier becomes larger when the positive polarization reverses to the negative state. This is due to the fact that the depolarization field and the built-in field are in the same direction and can be evidence of the existence of a positive built-in field, which makes the negative polarization state less stable. With decreasing compressive strain, we can see a gentler slope of the macroscopic-averaged electrostatic potential energy profile but a slightly larger average height of the potential barrier.

This might indicate a larger electroresistance of the tunnel junction with a small compressive strain, and the change of electroresistance with different metal electrodes might forecast an electrode-controlled GPR effect.

Since our primary concerns are the interfacial M–O bond, the epitaxial strain and their joint effect, the effect of the built-in field and terminations should be eliminated. We thus further calculate the entirely symmetric FTJs by changing electrode 2 from SRO to a metal. Without the difference between work functions of the two interfaces, the double-well profile is symmetrical with two polarization directions (see Fig. S3, ESI†). Similar to the A-FTJs, the electrode control is

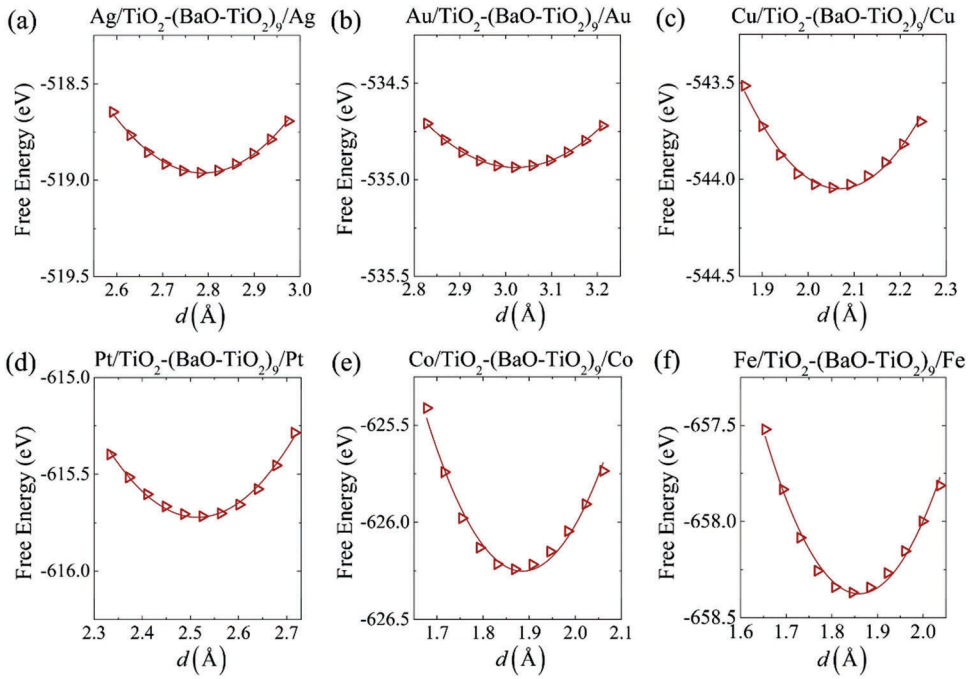

Fig. 11 The M–O binding energy *vs.* M–O bond length for the M/TiO_2–(BaO–TiO_2)$_9$/M S-FTJs under −3% strain.

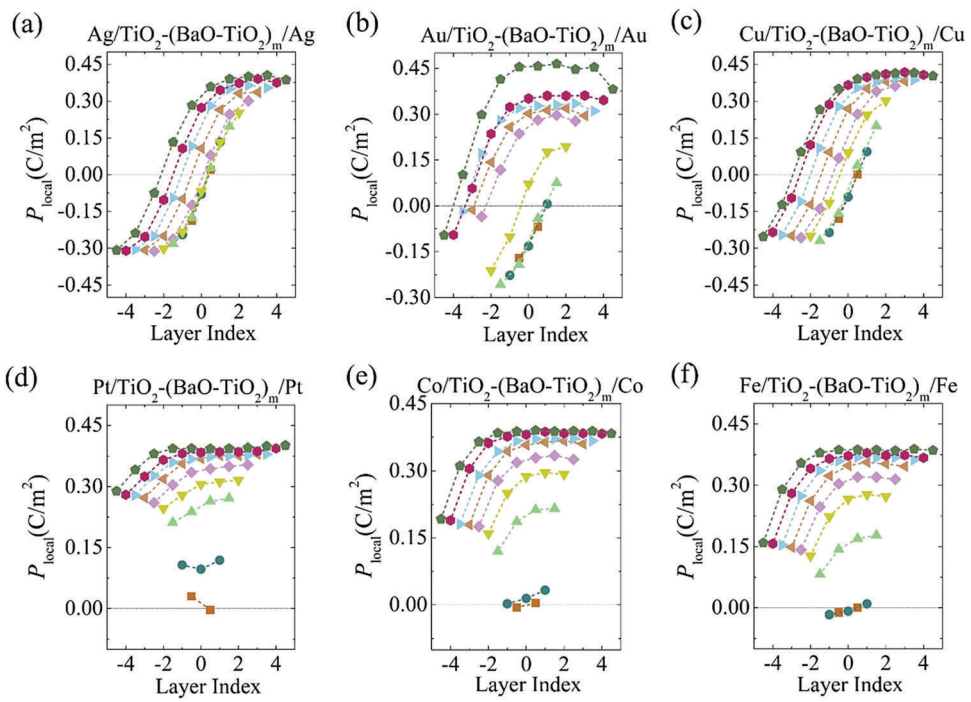

Fig. 12 The local polarization distribution of the M/TiO_2–(BaO–TiO_2)$_m$/M S-FTJs with *m* ranging from 2 to 10 under −3% strain. The layer index is set zero at the middle plane of the barrier.

studied by calculating the M–O binding energy *vs.* M–O bond length for symmetric M/TiO_2–$(BaO–TiO_2)_9$/M junctions under −3% strain. The results are depicted in Fig. 11(a–f). It can be seen that with the same change of bond length d, the parabolas of Ag–O and Au–O are gentle with k = 7.97 and 6.05, respectively. While those of Co–O and Fe–O are steeper with k = 18.25 and 19.23, respectively. Cu–O and Pt–O are in the middle class. These results are similar with those of the A-FTJs, indicating a negligible influence of different terminations on the M–O bond strength. When calculating the local polarization distributions, we give all BTO unit cells an initial ferroelectric distortion pointing from interface 1 to interface 2 before structural relaxation. This uniform initial ferroelectric distortion direction leads to a short distance between metal and oxygen atoms at interface 1 but a long distance at interface 2. Local polarization distributions shown in Fig. 12 indicate that the M–O bond length becomes much shorter at interface 1 after relaxation. Despite of this shortening phenomenon, Pt/$(TiO_2$–$BaO)_9$–TiO_2/Pt, Co/$(TiO_2$–$BaO)_9$–TiO_2/Co and Fe/$(TiO_2$–$BaO)_9$–TiO_2/Fe junctions still remain at the initial polarization state. However, in M_w/$(TiO_2$–$BaO)_9$–TiO_2/M_w junctions, polarization reversal happens near interface 1. This difference could originate from the stronger bond strength of Pt–O, Co–O and Fe–O, which makes the atoms difficult to move far from the initial displacement. Meanwhile, the Ag–O, Au–O and Cu–O bonds have inclination to get shorter in order to form more stable states. This distinction is well consistent with the results of the M–O bonds in the A-FTJs.

The strain control on symmetric tunnel junctions is also calculated. Note that there may exist counteraction of positive and negative polarizations in some junctions. The average polarization cannot provide accurate information. Therefore, we substitute the local polarization profile for the average polarization under each strain state to investigate the strain effect on the M/FTF interface in the S-FTJs, as presented in Fig. 13. Since compressive strain can enlarge the average Ti–O rumpling in the whole junction, it is easy to understand that the negative polarization decreases with decreasing compressive strain from −3% to −1%. This process is also accompanied by

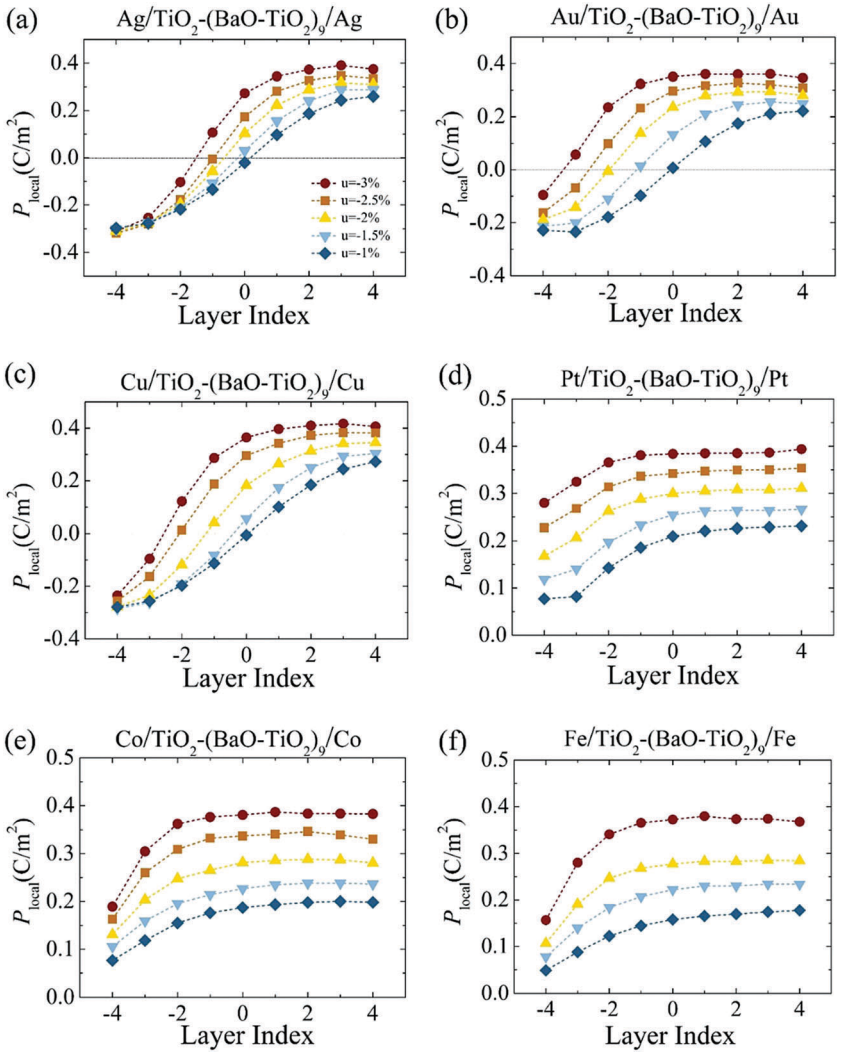

Fig. 13 The local polarization profile of the M/TiO_2–$(BaO–TiO_2)_9$/M S-FTJs under strain ranging from −3% to −1%. The layer index is set zero at the middle plane of the barrier.

an increase in the number of unit cells with a positive ferroelectric distortion near the interface 1 of $M_w/(TiO_2–BaO)_9–TiO_2/M_w$ tunnel junctions, leading to a decrease in depolarization field (see Fig. S4, ESI†). When −1% strain is applied, the negative polarization in these three junctions is even completely neutralized, forming a paraelectric-like state.

E. Discussion

Our results provide us guidance on practical applications of the FTJs with regard to the selection of electrodes and substrates. In practical applications, requirements on the performance of the FTJs can be varied. For example, to exploit the GER effect, an enhanced polarization asymmetry that can bring a large difference in the electroresistance of the two polarization states is desirable. For memory applications, a strong polarization bi-stability with a small critical thickness would be the best choice. According to the finding of our study, for applications of $M/(TiO_2–BaO)/SRO$ FTJs in the cases where strong polarization bi-stability is needed, choosing M_s (such as Pt, Co and Fe) as an electrode, together with choosing substrates that can bring a greater compressive misfit strain, should be more suitable. In contrast, for applications where an enhanced polarization asymmetry is needed, it is recommended to select M_w (such as Ag, Cu and Au). In addition, the choice of electrodes and substrates will significantly affect the value of polarization in the FTJs. According to our results, the largest polarization can be achieved with a Cu electrode while the smallest polarization is achieved with a Pt electrode in the asymmetric FTJs. With strain ranging from −1% to −3%, the largest polarization can be achieved under −3% strain (for example, depositing BTO thin films on a $LaAlO_3$ substrate). Therefore, for applications where a large value of polarization is required, it would be better to choose the Cu electrode, together with substrates that can bring a greater compressive misfit strain.

Conclusions

In conclusion, we have investigated the electrode and strain control on the ferroelectric polarization bi-stability in both A-FTJs and S-FTJs utilizing the *ab initio* simulations. More than 1000 FTJ structures were calculated in this work. 6 commonly used metals, Au, Ag, Cu, Pt, Co and Fe, and also the SRO oxide are chosen as electrodes. In all junctions, the number of BTO layers ranges from 2 to 10. Both positive and negative initial ferroelectric distortions are considered during the calculations. The strain effect is taken into account by further calculating all the A-FTJs and S-FTJs under −3%, −2.5%, −2%, −1.5% and −1% strain. Through calculation of the M–O bond strength k and the double-well energy profile in both A-FTJs and S-FTJs, the six metal electrodes can be divided into two classes. In competition with the effect of the built-in field, the interfacial M–O bond has a strong modulation on the polarization bi-stability of a tunnel junction. The weaker bonds M_w–O with Ag, Au and Cu electrodes show an enhancement of the positive ferroelectric polarization while the stronger bonds M_s–O including Pt–O, Co–O and Fe–O bonds tend to stabilize the negative polarization state. With decreasing compressive strain, the critical thickness of the bi-stable polarization increases. This combined effect of the electrode and strain control provides a free modulation of the polarization state, and 'mechanical switching' of the metastable polarization state can be achieved. The last but not the least, the change of electroresistance with different metal electrodes under different strains might forecast an electrode-controlled GPR effect which we hope to investigate both theoretically and experimentally in the future.

Acknowledgements

This work was supported by NSFC (No. 11474363, 11602310, 11672339). Yue Zheng also acknowledges the support from the Special Program for Applied Research on Super Computation of the NSFC-Guangdong Joint Fund (the second phase), the Fok Ying Tung Foundation, the Guangdong Natural Science Funds for Distinguished Young Scholar and the China Scholarship Council.

References

1 H. Kohlstedt, N. Pertsev, J. R. Contreras and R. Waser, *Phys. Rev. B: Condens. Matter Mater. Phys.*, 2005, **72**, 125341.
2 M. Y. Zhuravlev, R. F. Sabirianov, S. Jaswal and E. Y. Tsymbal, *Phys. Rev. Lett.*, 2005, **94**, 246802.
3 E. Y. Tsymbal and H. Kohlstedt, *Science*, 2006, **313**, 181.
4 A. Chanthbouala, V. Garcia, R. O. Cherifi, K. Bouzehouane, S. Fusil, X. Moya, S. Xavier, H. Yamada, C. Deranlot and N. D. Mathur, *Nat. Mater.*, 2012, **11**, 860.
5 A. Chanthbouala, A. Crassous, V. Garcia, K. Bouzehouane, S. Fusil, X. Moya, J. Allibe, B. Dlubak, J. Grollier and S. Xavier, *Nat. Nanotechnol.*, 2012, **7**, 101.
6 V. Garcia, S. Fusil, K. Bouzehouane, S. Enouz-Vedrenne, N. D. Mathur, A. Barthelemy and M. Bibes, *Nature*, 2009, **460**, 81.
7 A. Gruverman, D. Wu, H. Lu, Y. Wang, H. Jang, C. Folkman, M. Y. Zhuravlev, D. Felker, M. Rzchowski and C.-B. Eom, *Nano Lett.*, 2009, **9**, 3539.
8 M. Y. Zhuravlev, S. Jaswal, E. Y. Tsymbal and R. F. Sabirianov, *Appl. Phys. Lett.*, 2005, **87**, 222114.
9 J. P. Velev, C.-G. Duan, J. Burton, A. Smogunov, M. K. Niranjan, E. Tosatti, S. Jaswal and E. Y. Tsymbal, *Nano Lett.*, 2008, **9**, 427.
10 V. Garcia, M. Bibes, L. Bocher, S. Valencia, F. Kronast, A. Crassous, X. Moya, S. Enouz-Vedrenne, A. Gloter and D. Imhoff, *Science*, 2010, **327**, 1106.
11 M. Hambe, A. Petraru, N. A. Pertsev, P. Munroe, V. Nagarajan and H. Kohlstedt, *Adv. Funct. Mater.*, 2010, **20**, 2436.
12 D. Kim, J. Jo, Y. Kim, Y. Chang, J. Lee, J.-G. Yoon, T. Song and T. Noh, *Phys. Rev. Lett.*, 2005, **95**, 237602.
13 G. Gerra, A. Tagantsev, N. Setter and K. Parlinski, *Phys. Rev. Lett.*, 2006, **96**, 107603.
14 J. Junquera and P. Ghosez, *Nature*, 2003, **422**, 506.
15 M. A. M. Polanco, I. Grinberg, A. M. Kolpak, S. V. Levchenko, C. Pynn and A. M. Rappe, *Phys. Rev. B: Condens. Matter Mater. Phys.*, 2012, **85**, 214107.

16 N. Sai, A. M. Kolpak and A. M. Rappe, *Phys. Rev. B: Condens. Matter Mater. Phys.*, 2005, **72**, 020101.
17 A. Tagantsev and G. Gerra, *J. Appl. Phys.*, 2006, **100**, 051607.
18 M. Stengel, D. Vanderbilt and N. A. Spaldin, *Nat. Mater.*, 2009, **8**, 392.
19 W. Chen, Y. Zheng, X. Luo, B. Wang and C. Woo, *J. Appl. Phys.*, 2013, **114**, 064105.
20 X. Liu, Y. Wang, P. V. Lukashev, J. D. Burton and E. Y. Tsymbal, *Phys. Rev. B: Condens. Matter Mater. Phys.*, 2012, **85**, 125407.
21 H. Lu, X. Liu, J. Burton, C. W. Bark, Y. Wang, Y. Zhang, D. Kim, A. Stamm, P. Lukashev and D. Felker, *Adv. Mater.*, 2012, **24**, 1209.
22 D. G. Schlom, L.-Q. Chen, C.-B. Eom, K. M. Rabe, S. K. Streiffer and J.-M. Triscone, *Annu. Rev. Mater. Res.*, 2007, **37**, 589.
23 S. Sahoo, S. Polisetty, C.-G. Duan, S. S. Jaswal, E. Y. Tsymbal and C. Binek, *Phys. Rev. B: Condens. Matter Mater. Phys.*, 2007, **76**, 092108.
24 X. Luo, S. Lin, B. Wang and Y. Zheng, *Appl. Phys. Lett.*, 2010, **97**, 012905.
25 Y. Zheng and C. Woo, *Nanotechnology*, 2009, **20**, 075401.
26 H. Lu, C.-W. Bark, D. E. De Los Ojos, J. Alcala, C.-B. Eom, G. Catalan and A. Gruverman, *Science*, 2012, **336**, 59.
27 W. Chen, Y. Zheng, X. Feng and B. Wang, *J. Mech. Phys. Solids*, 2015, **79**, 108.
28 X. Luo, B. Wang and Y. Zheng, *ACS Nano*, 2011, **5**, 1649.
29 G. Kresse, J. Furthmüller and J. Hafner, *EPL*, 1995, **32**, 729.
30 P. E. Blöchl, *Phys. Rev. B: Condens. Matter Mater. Phys.*, 1994, **50**, 17953.
31 J. P. Perdew and A. Zunger, *Phys. Rev. B: Condens. Matter Mater. Phys.*, 1981, **23**, 5048.
32 H. J. Monkhorst and J. D. Pack, *Phys. Rev. B: Condens. Matter Mater. Phys.*, 1976, **13**, 5188.
33 R. King-Smith and D. Vanderbilt, *Phys. Rev. B: Condens. Matter Mater. Phys.*, 1993, **47**, 1651.
34 X. Luo, Y. Zheng and B. Wang, *J. Appl. Phys.*, 2012, **111**, 074102.
35 I. Oleinik, E. Y. Tsymbal and D. Pettifor, *Phys. Rev. B: Condens. Matter Mater. Phys.*, 2001, **65**, 020401.